

UNIVERSITY of CALIFORNIA
SANTA CRUZ

**ANALYSIS OF THE TGF OBSERVATION MADE BY THE
AIRBORNE DETECTOR FOR ENERGETIC LIGHTNING
EMISSIONS**

A thesis submitted in partial satisfaction of the
requirements for the degree of

BACHELOR OF SCIENCE

in

PHYSICS

by

Alexander W. Lowell

10 June 2010

The thesis of Alexander W. Lowell is approved by:

Professor David M. Smith
Advisor

Professor David P. Belanger
Senior Theses Coordinator

Professor David P. Belanger
Chair, Department of Physics

Copyright © by

Alexander W. Lowell

2010

Acknowledgements

Thanks to David Smith, Bryna Hazelton, Brian Grefenstette, Nicole Kelley, Forest Martinez-McKinney, and Zi Yan Zhang for their patience and helpfulness!

Abstract

Observations of high-energy activity above thunderstorm systems were made by the Airborne Detector for Energetic Lightning Emissions (ADELE) in August and September 2009. One Terrestrial Gamma-Ray Flash (TGF) was observed on August 21, 2009 with no associated lightning discharge. The lack of TGFs in the ADELE data set was unexpected, since TGFs were believed to be closely associated with lightning, and ADELE flew by many lightning discharges.

Monte Carlo simulations of TGFs in the atmosphere were used to determine the spatial regions in the atmosphere in which ADELE should have detected a TGF. The “cutoff” horizontal distance from the TGF source point where the TGF was no longer “detectable” (with respect to the ADELE instrument) was found as a function of TGF source altitude, assuming a constant airplane altitude of 13.5 km. Lightning data provided by lightning detection networks facilitated the search for lightning flashes within the ADELE cutoff distances. The data sets provided by the lightning detection networks indicate that there were many lightning flashes within the ADELE cutoff distances. This leads us to hypothesize that most lightning does not produce TGFs, and that perhaps lightning and TGFs are not mutually inclusive.

Contents

| | | |
|----------|---|-----------|
| 1 | Introduction | 2 |
| 1.1 | Background | 2 |
| 1.2 | TGF Characteristics | 6 |
| 1.3 | TGF production mechanism | 8 |
| 1.4 | The Airborne Detector for Energetic Lightning Emissions | 10 |
| 1.5 | Summer 2009 Flight Campaign | 12 |
| 2 | Monte Carlo Simulations | 16 |
| 2.1 | GEANT | 16 |

| | | |
|----------|--|-----------|
| 2.2 | Characterization of the ADELE instrument sensitivity | 17 |
| 2.3 | Simulation of TGFs in the atmosphere | 18 |
| 3 | Results | 21 |
| 4 | Discussion | 22 |
| 5 | References | 24 |

1 Introduction

1.1 Background

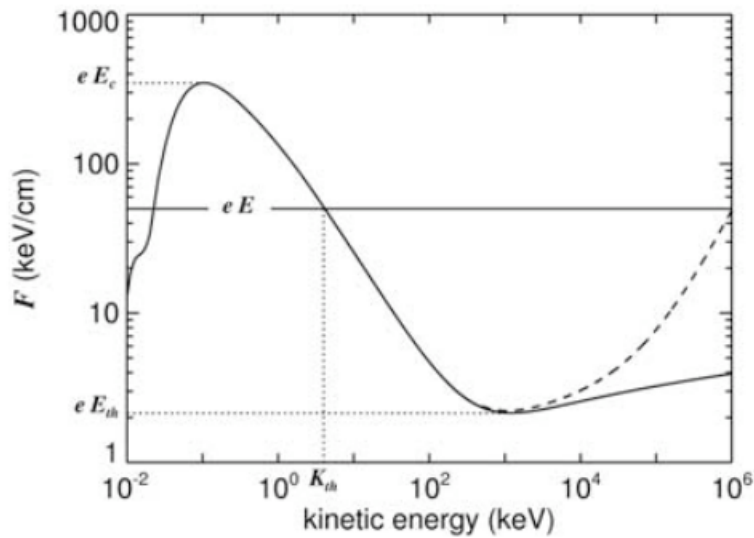


Figure 1: Drag force on electrons in air as a function of electron energy. The dashed line includes the energy losses due to bremsstrahlung emission, while the solid line only includes inelastic scattering of electrons off of air. Taken from Dwyer (2004).

High-energy emissions from thunderstorm systems were first predicted by C.T.R. Wilson (1925) by noting that the drag force due to air as a function of electron energy has a maximum as depicted in Fig. 1. Thus, electrons with energy greater than some threshold energy (determined by the intersection of the drag force curve with the line of constant electric field strength) will be accelerated by the electric field to relativistic energies. These “runaway electrons” may knock electrons off molecules in the air and give these electrons energies greater than the threshold energy required for runaway. In this way, an avalanche of runaway electrons may occur, producing bremsstrahlung radiation upon impact with molecules in the air.

The first convincing measurements of this radiation were made in the early eighties with NaI scintillation detectors flown through thunder clouds (Parks, 1981; McCarthy and Parks, 1985). X-ray surges lasting on the order of seconds were observed, with count rates exceeding the background rates by almost two orders of magnitude. Interestingly, the surges appeared to turn off in conjunction with nearby lightning flashes. Figure 2 shows the count rates (for photons with energy between 5.5 keV and 110 keV) as a function of time along with the coincident lightning flashes.

The instrument used by Parks and McCarthy was only sensitive to photons up to 110 keV and thus was incapable of resolving higher energy photons. Wilson had hypothesized that electrons produced via the electron avalanche mechanism would have energies up into the GeV range; electrons with such high energies would produce photons with energies well above 110 keV. Confirmation of higher-energy radiation was made with the discovery of Terrestrial Gamma-Ray Flashes (TGFs) in 1994 by the Burst and Transient Source Experiment

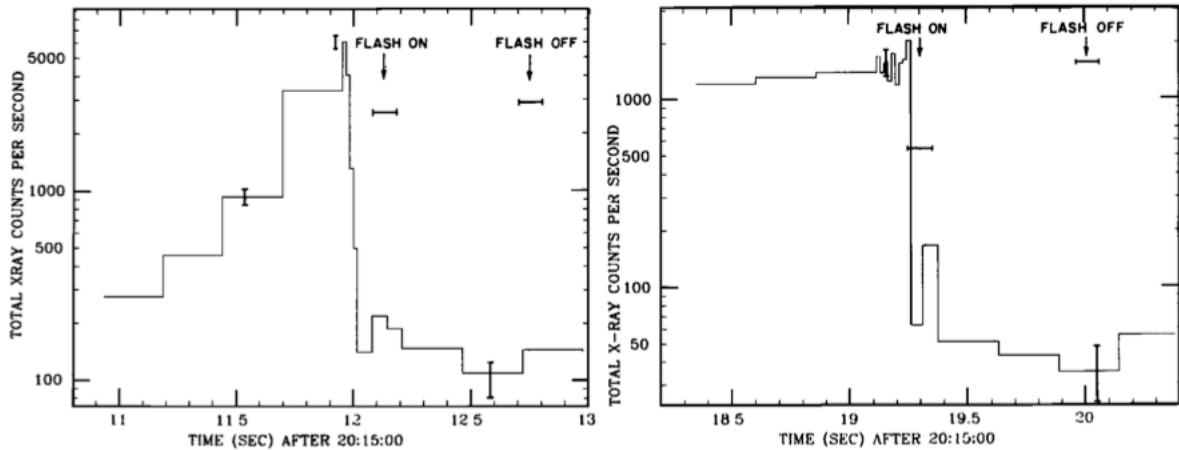


Figure 2: Count rates as a function of time for energies between 5.5 keV and 110 keV. Taken from McCarthy and Parks (1985).

(BATSE) aboard the Compton Gamma-Ray Observatory (CGRO) satellite.

The BATSE instrument was designed to make gamma-ray observations from space with its 8 NaI scintillation detectors positioned at the corners of the satellite. The geometry of the detector arrangement allowed for all-sky monitoring. Additionally, the direction from which the photons were arriving was inferred by comparing the responses of the detectors.

The discovery of TGFs by BATSE was unexpected, since there was no reason to believe that strong bursts of gamma-rays should be coming from the direction of the earth. Fishman et al. (1994) noted that the BATSE triggers corresponding to the strange, millisecond-long events from the earthward direction happened to coincide with thunderstorm activity in the sub-satellite zone. These triggers were more rare than typical BATSE triggers, since BATSE was not designed to trigger on time scales shorter than 64 milliseconds.

Evidence supporting a correlation between TGFs and lightning discharges was first presented by Inan et al. (1996) when a spheric, the characteristic radio wave generated by

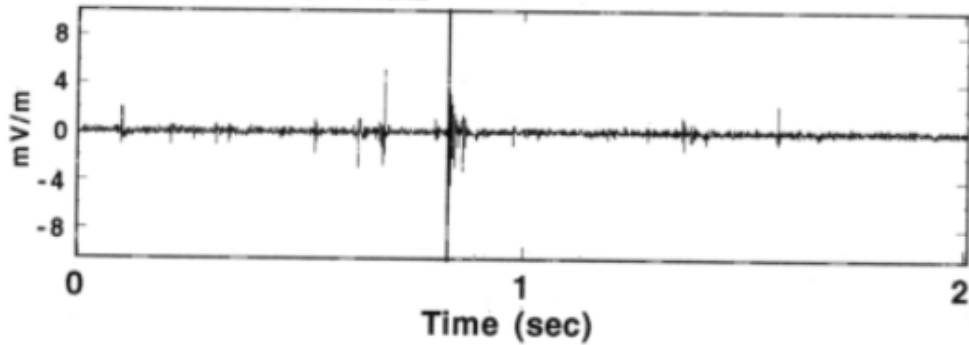


Figure 3: Raw time series sferic data for BATSE event 2348. Frequencies above 1 kHz were filtered out for this plot. Taken from Inan (1996).

lightning, was shown to coincide with BATSE TGF number 2348. Figure 4 shows BATSE event 2348 while Fig. 3 shows the corresponding sferic, detected at the Palmer Station in Antarctica. Since then, many TGFs have been found to have corresponding sferics, thus strengthening the link between lightning and TGFs.

In 2002, the Reuven Ramaty High Energy Solar Spectroscopic Imager (RHESSI) satellite was launched and has since been responsible for the majority of TGF observations. RHESSI is equipped with nine germanium detectors which offer better energy and time resolution than the NaI scintillation detectors found on BATSE, allowing for more detailed analysis of TGF spectra. Moreover, RHESSI continuously records every photon and does not depend on a trigger algorithm for data collection (Smith et al., 2005). This leads to a much larger TGF detection rate than that found with BATSE (approximately 10-15 TGFs per month, compared to BATSE's 1 TGF per two months). The RHESSI TGF detection rate along with the low-earth orbit of the RHESSI satellite has (on few occasions) led to separate TGF observations made on different passes over the same storm system, further supporting the hypothesis that TGFs originate from thunderstorm activity.

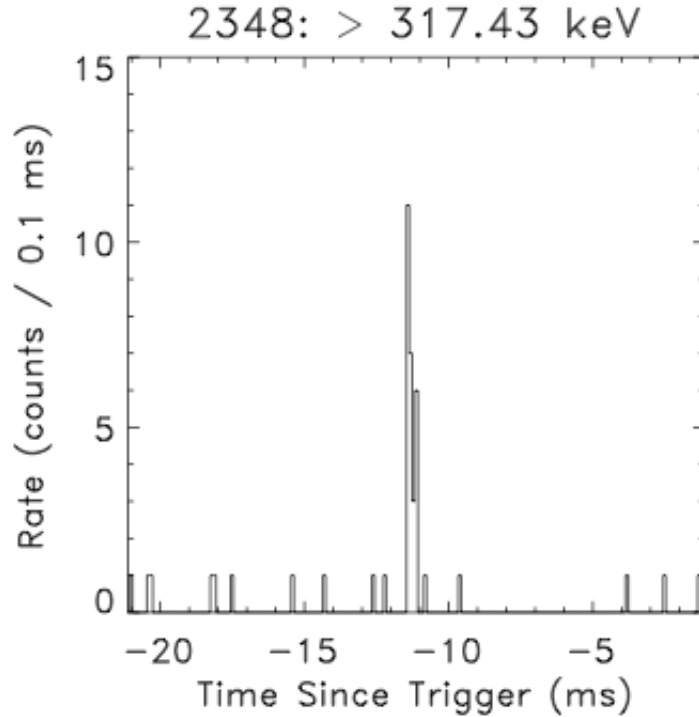


Figure 4: BATSE event 2348, summed over all triggered detectors for photon energies >317 keV. Taken from Mallozzi (2002).

1.2 TGF Characteristics

TGFs are intense bursts of x-rays and gamma-rays that originate from the atmosphere. The TGF source altitude is unknown, but has been inferred from a comparison between RHESSI data and monte carlo simulations to be between 15 and 21 km (Dwyer & Smith, 2005). Figure 5 shows time profiles for 4 RHESSI TGFs, while Figure 6 shows time profiles for 12 BATSE TGFs. As is evident from the figures, TGFs can have one or more peaks and last between .5 and 3.5 milliseconds.

Typical TGFs seen by RHESSI consist of relatively few counts (usually between 18 and 100 counts). So in order to get a better idea of the spectral characteristics, a summed

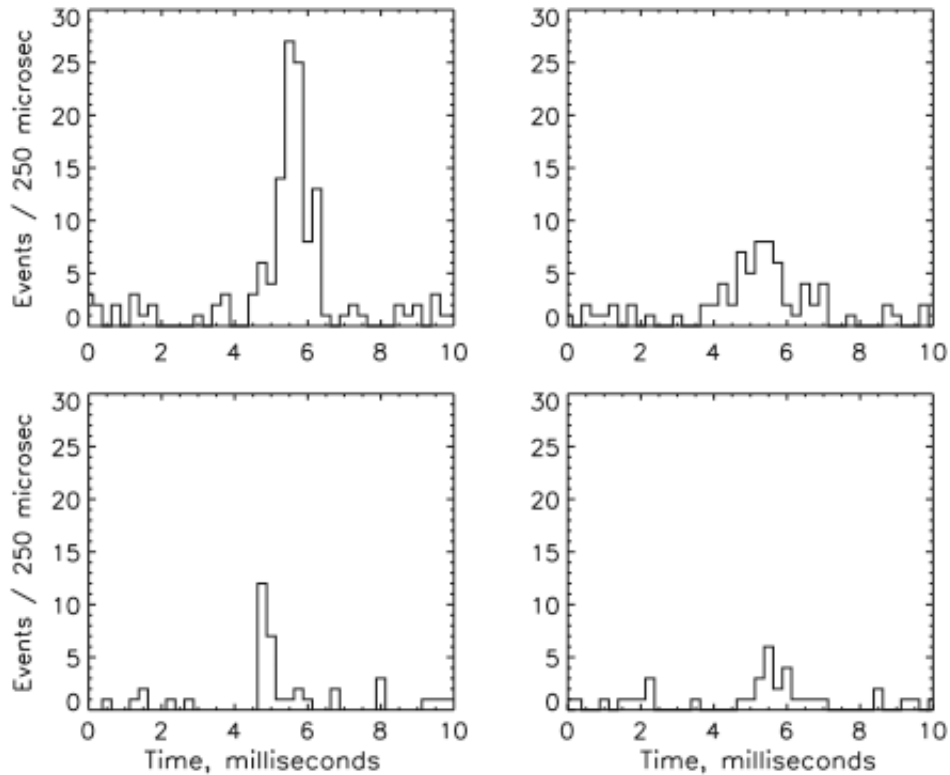


Figure 5: Time profiles for 4 typical RHESSI TGFs, from Smith et al. (2005).

spectrum is used. Figure 7 shows a summed spectrum of 289 RHESSI TGFs. The hump centered about 100 keV corresponds to photons that have undergone Compton scattering in the atmosphere. These photons tend to arrive after the higher energy photons since their paths are longer due to the scattering (Grefenstette et al., 2008). The higher energy portion of the spectrum is consistent with bremsstrahlung radiation with a characteristic energy of 7 MeV. The lower end of the spectrum flattens out due to photoelectric absorption in the atmosphere, which has a larger cross-section for lower energy photons.

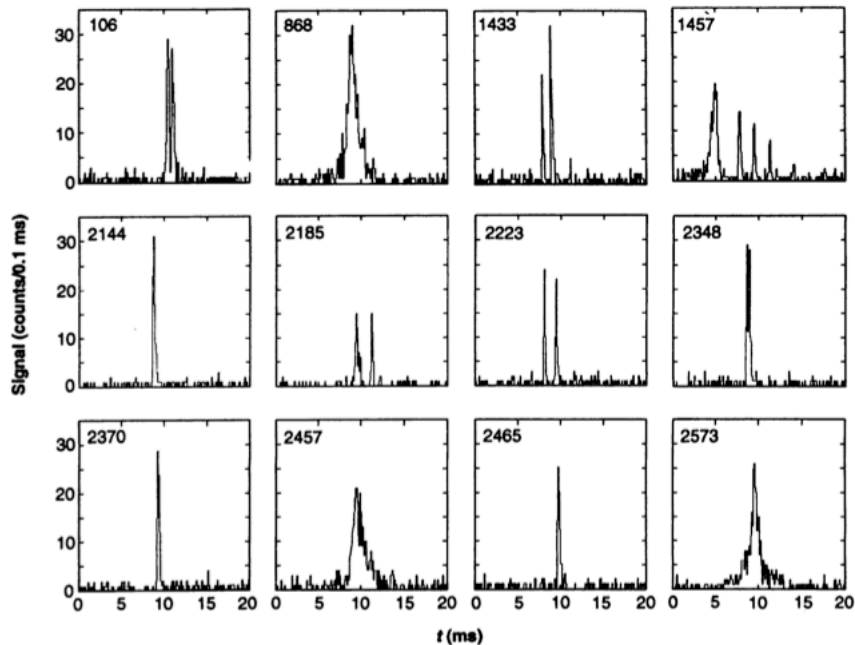


Figure 6: Time profiles for 12 typical BATSE TGFs. The BATSE trigger algorithm often triggers on multi-peaked TGFs, whereas the RHESSI TGF search algorithm does not often see multi-peaked TGFs. Taken from Fishman et al. (1994).

1.3 TGF production mechanism

The exact mechanism for TGF initiation is still a matter of theoretical debate. The relativistic runaway electron avalanche (RREA) mechanism described earlier is likely to play a key role in the process. In order to produce an RREA, a seed electron with energy above the runaway threshold must enter the electric field region. The observed luminosities of TGFs imply that a large number of RREAs must be taking place in the electric field region; one seed electron initiating one RREA does not produce enough photons for a TGF.

One possibility is that some physical process is generating a large population of energetic seed electrons which encounter the field region and produce enough RREAs for a TGF. The mechanism of “Cold Runaway” in lightning leader tips (Moss et al., 2006) is a likely

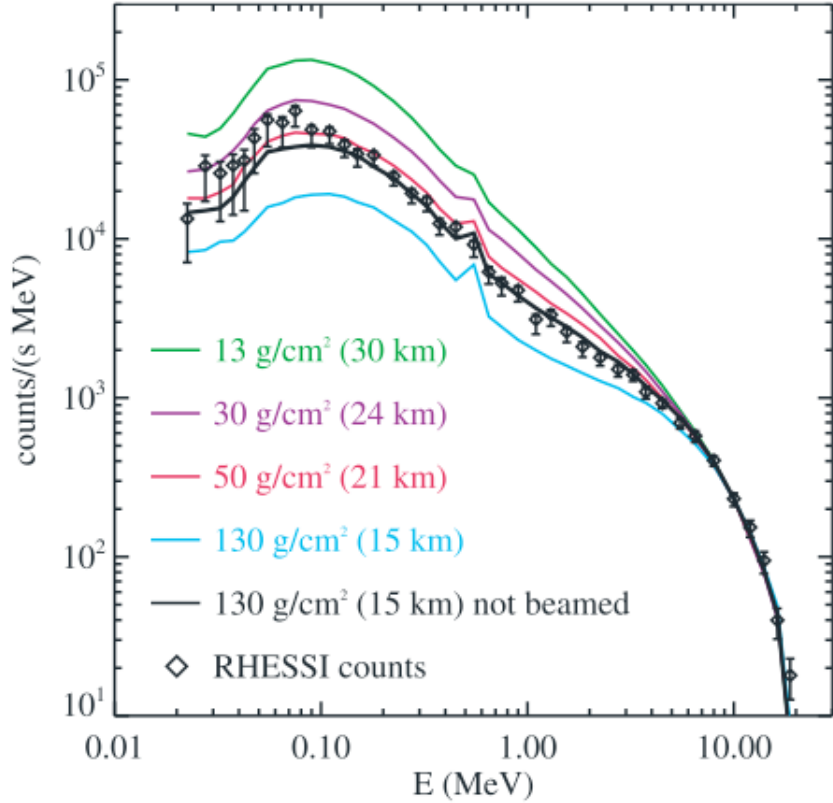


Figure 7: A summed spectrum of 289 RHESSI TGFs. The Diamonds correspond to the raw RHESSI data. The other curves represent spectra produced by simulations of what RHESSI would see for different TGF source altitudes, with the instrumental response taken into account. Taken from Dwyer & Smith (2005)

candidate for such a physical process. In this model, the electric fields produced at the tips of lightning leaders are so intense that they will cause electrons with any energy to run away. This would correspond to a line of constant electric field larger than the drag force for all energies in Fig. 1. However, since the field region in the leader tips is not very large, the electrons are not necessarily accelerated to relativistic energies. These semi-energetic electrons may encounter the primary electric field region in the thunder cloud where their energies exceed the threshold for relativistic runaway, thus resulting in RREAs.

The “Positron Feedback” model (Dwyer, 2008) is another theory that aims to explain the source of the seed electrons necessary for a TGF. In this model, only one seed electron is needed. Upon entering the field region, the electron runs away and produces an RREA. The bremsstrahlung photons produced by the RREA with energies >1.22 MeV may produce electron-positron pairs. The electrons continue to travel against the field lines, while the positrons travel in the opposite direction. The positrons may encounter air molecules and produce knock-on electrons that may then run away and start the positron feedback process over again.

1.4 The Airborne Detector for Energetic Lightning Emissions

TGF observations made by RHESSI are limited in two ways. First, the germanium detectors are saturated by most TGF events, effectively obscuring the true count rates (Grefenstette, 2009). Second, RHESSI would be incapable of detecting weak TGFs or TGFs that originate deep in the atmosphere due to atmospheric attenuation. Of course this would be true for any detectors in orbit, not just RHESSI. This means that TGF observations made from orbit may only be addressing a subset of the TGF family, corresponding to the strongest or highest-altitude TGFs.

In order to better understand the TGF phenomenon, the Airborne Detector for Energetic Lightning Emissions (ADELE) was built at UCSC for TGF observations from primarily airplane altitudes, but also from the ground. ADELE consists of two NaI scintillation detectors and four plastic scintillation detectors. The signals from the plastic detectors are binned into four coarse energy channels (>50 keV, >300 keV, >1 MeV, >5 MeV, digitized by an FPGA,

and continuously stored on a computer. Statistically significant variations in count rates seen by the plastic detectors trigger data collection from the NaI detectors, which offer much better energy resolution and allow for spectral data analysis. The signal from a flat plate antenna mounted on the bottom of the airplane fuselage is also recorded with this trigger so that the count rate data can be compared to the local variations in the electric field. A picture of ADELE fully constructed and mounted in a rack is shown in Fig. 8.



Figure 8: The ADELE instrument. The upper and lower sensor heads are clearly visible.

The scintillation detectors are divided into an upper and a lower "sensor head," as can be seen in Fig. 8. The tops of the scintillators in the lower sensor head and the bottoms of the scintillators in the upper sensor head are shielded with lead plates, thus allowing for a

rough up/down signal discrimination. The ratio between the upper signal and lower signal can be used for a rough inference of the TGF location.

Each sensor head has one 5" NaI detector, one 5" plastic detector, one 1" plastic detector, and an empty detector tube used as a control. The NaI detectors have a large dead time and high stopping power, so they are most useful in low count-rate situations. For higher count-rate situations, the plastic detectors are more useful, as they have a smaller dead time and less stopping power than the NaI detectors. For extremely high count rates, the 5" plastic detectors may saturate while the 1" detectors may not by virtue of their smaller size. This combination of detectors gives ADELE a wide dynamic range for observations of high-energy activity. This is an important feature of ADELE since the luminosities and source altitudes of TGFs are uncertain and have never been measured from within the atmosphere.

1.5 Summer 2009 Flight Campaign

Construction of the ADELE instrument was completed in July of 2009, and flights aboard the National Center for Atmospheric Research airplane, a Gulfstream V, were carried out through mid to late August of 2009. A total of 37 flight hours were logged over the Southeastern United States, typically during the late afternoons and evenings, since these are the most likely times for thunderstorm activity. The plane was flown above and around electrically active thunder clouds, although flight through the clouds was forbidden due to safety regulations. On one occasion (August 21, 2009), the plane was accidentally flown through the top of a thunder cloud, resulting in a sudden loss of altitude and a huge spike in count rates lasting for a couple of seconds (qualifying it as a surge). This event is shown

in Fig. 9.

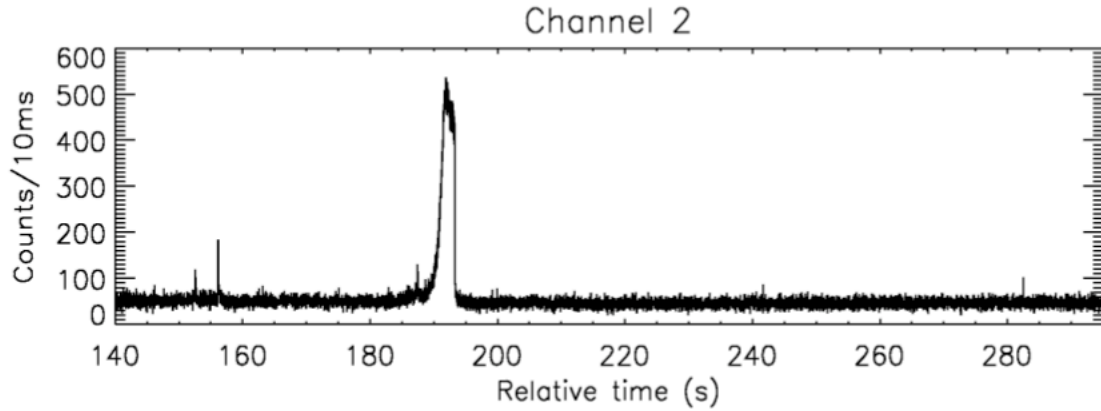


Figure 9: Large surge event from August 21, 2009. The small spike just after $t = 280$ s is the TGF.

Following the operations, the data from the plastic detectors were searched for TGF signatures. The algorithm used for this search compared the 2nd energy channels (>300 keV) of the 5" plastic detectors and looked for coincidental events above a statistical threshold, while screening out counts due to cosmic rays. After searching through the entire data set, only one TGF matching the search criteria was found.

The TGF occurred on August 21, 2009 at approximately 20:14:43.437, just 90 seconds after the surge event mentioned earlier. Figure 10 shows a time profile of the TGF event, while Table 1 shows the amount of counts in each energy channel for the top and bottom 5" plastic detectors. Additionally, the TGF is just barely visible off to the right in Fig. 9. The TGF was relatively weak and did not trigger collection of the NaI detector and flat plate antenna data. As a result, detailed spectral data and electric field data are not available for the event.

Positional lightning flash data provided by the Los Alamos Sferic Array (LASA) was

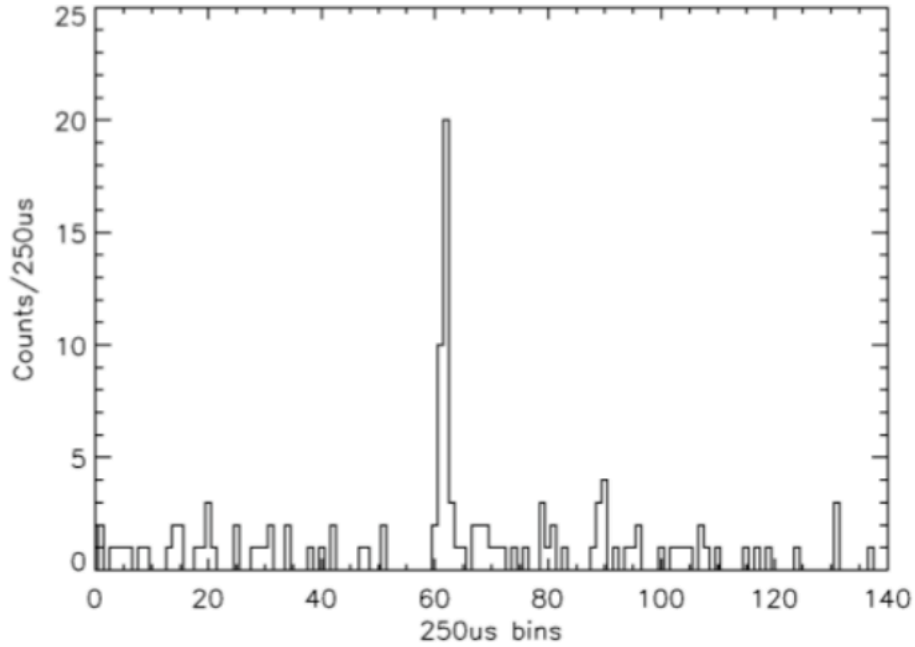


Figure 10: The only TGF from the entire flight campaign.

| Detector | Ch. 1 | Ch. 2 | Ch. 3 | Ch. 4 |
|----------|----------|-----------|-----------|----------|
| Upper | 77 (3.5) | 26 (0.83) | 9 (0.52) | 3 (0.44) |
| Lower | 52 (4.2) | 18 (0.91) | 10 (0.60) | 1 (0.51) |

Table 1: Counts deposited in 5" plastic detectors by the TGF. The quantities in parentheses are the average counts in a millisecond for the entire campaign.

searched for lightning flashes that occurred at the same time as the TGF. The lightning detection networks require that the sferics emitted by a lightning flash register on at least two of their detectors in order to triangulate the flash position. Unfortunately, only a small blip was seen at one LASA station (Tallahassee, FL) consistent with the timing of the observed TGF, depicted in Fig. 11. Thus we cannot say with certainty that the TGF had an associated lightning discharge near the instrument.

The lightning data also indicate that there were many flashes near the airplane's position

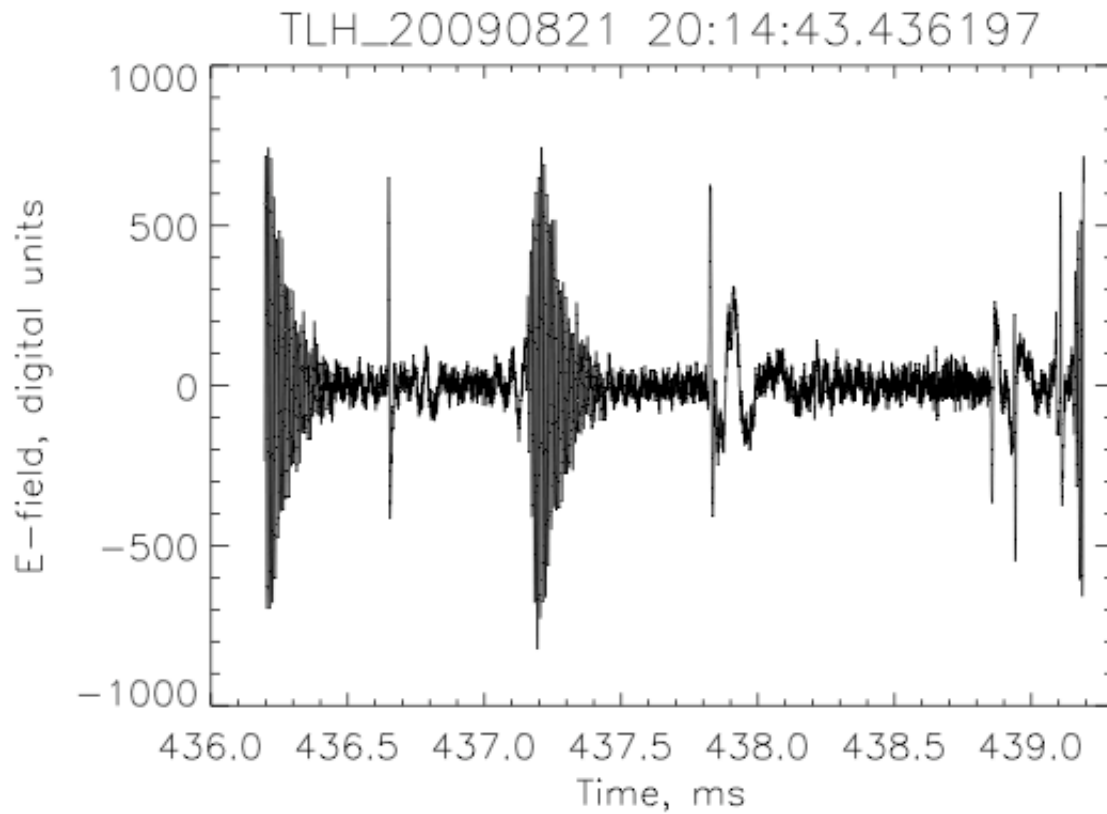


Figure 11: Sferic seen on the LASA Tallahassee, FL station. The orientation and frequency of the sferic indicates that it was associated with a positive, intracloud discharge. Courtesy of Xuan-Min Shao.

on practically every flight. The absence of TGFs from the data set thus leads to the hypothesis that most lightning does not produce TGFs, because if it did, ADELE would have detected them.

2 Monte Carlo Simulations

2.1 GEANT

The simulations discussed for the remainder of this thesis were written using GEANT3, a suite of monte carlo simulation tools written in FORTRAN that includes all of the relevant physical processes (photoelectric absorption, Compton scattering, bremsstrahlung emission, pair production, etc.) that take place as particles pass through matter (GEANT team, 1993).

The first step of any GEANT program is to define the “mass model”. The mass model is the geometrical universe through which the particles are allowed to propagate. GEANT provides a library of standard shapes (spherical shells, rectangular boxes, cylinders, etc.) from which the mass model is constructed. Additionally, the stopping power and atomic weights of the materials must be specified in order to calculate the cross-sections for physical processes.

Once the mass model has been defined, energetic particles are originated from some point in the mass model with some initial direction and energy. For each step in position of a particle, GEANT calculates the probabilities of physical interactions and invokes a random number generator to determine the fate of the particle. As the particles scatter throughout the geometry, they may enter regions of interest (such as a plastic detector), at which point their energies and angles with respect to some axis are recorded. Once a particle has lost enough energy such that its remaining energy is below some user-defined threshold, the particle is no longer tracked.

Two different simulations were carried out for the purposes of this paper. The following

is a discussion of each simulation.

2.2 Characterization of the ADELE instrument sensitivity

In the first simulation, a mass model of the ADELE instrument was bombarded with a typical TGF spectrum. A schematic representation of the ADELE mass model is shown in Fig. 12. The dimensions of the included components are accurate representations of the experimental configuration. Only a certain level of detail is represented, corresponding to the most important components (airplane fuselage, detectors, etc.).

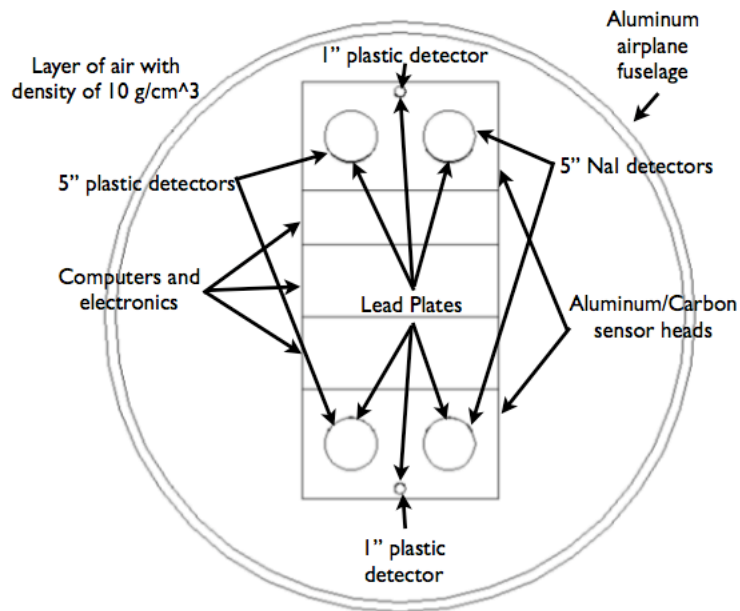


Figure 12: A schematic of the ADELE mass model used in this simulation.

Photons were chosen from a predetermined TGF spectrum and initialized on the surface of a sphere that encompassed the entire mass model. Of course, some of these photons would deposit energy in the detectors, and some would miss the detectors entirely. The number of

counts in the detectors was recorded and written to file at the end of the program.

In reality, some of the counts seen by ADELE were due to photons created by cosmic ray secondary interactions. The average number of counts per millisecond in channel 2 of the 5" plastic detectors on August 21 was $1.74 \frac{\text{counts}}{\text{ms}}$. The Poisson distribution with this mean value assigns a probability of $5.4\text{E-}10$ to observing a count rate of $15 \frac{\text{counts}}{\text{ms}}$ or more due to background. Multiplying this by the total number of one millisecond bins from the entire campaign yields a probability of 7% that one 1 millisecond bin would have 15 counts or more. Therefore, if the TGF search algorithm identifies a potential TGF event with $15 \frac{\text{counts}}{\text{ms}}$, then there is a 93% confidence interval that it was indeed a TGF.

So in order to determine the sensitivity of ADELE to a TGF event, the number of input photons N with energies >300 keV in the simulation was divided by the factor P , with $P = \frac{n}{15}$ and $n =$ number of photons absorbed in the 5" plastic detectors with energies >300 keV (this is the channel used by the TGF search algorithm). The ratio N/P was then divided by the cross-sectional area of the sphere used to initialize the photons, resulting in a minimum flux value at which ADELE would register a TGF (at a 93% confidence interval).

2.3 Simulation of TGFs in the atmosphere

Once the sensitivity of the ADELE instrument was determined, a second simulation was carried out in order to determine which spatial regions in the vicinity of a TGF would have photon fluxes exceeding the ADELE instrument sensitivity. The mass model for this simulation consisted of 48 concentric, spherical shells of air with varying densities, approximating the earth's atmosphere. Additionally, 66 identical detector volumes in the shape of disks

were placed in the atmosphere between the altitudes of 6.9 km and 19.9 km, centered on the z axis. These detector volumes had no physical analogue; their densities matched the density of the spherical air shell in which they laid. Their purpose was to count the photons that crossed their boundaries without altering any of the physics. A schematic representation of the mass model is shown in Fig. 13 . Each disk had a radius of 20 km and was subdivided into 40 rings, as shown in Fig. 13. One of the disks was positioned at an altitude of 13.5 km, corresponding to the average altitude of the GV airplane. This disk was of particular importance, as it was used to determine the maximum horizontal distance at which a TGF would still be detectable at the airplane altitude.

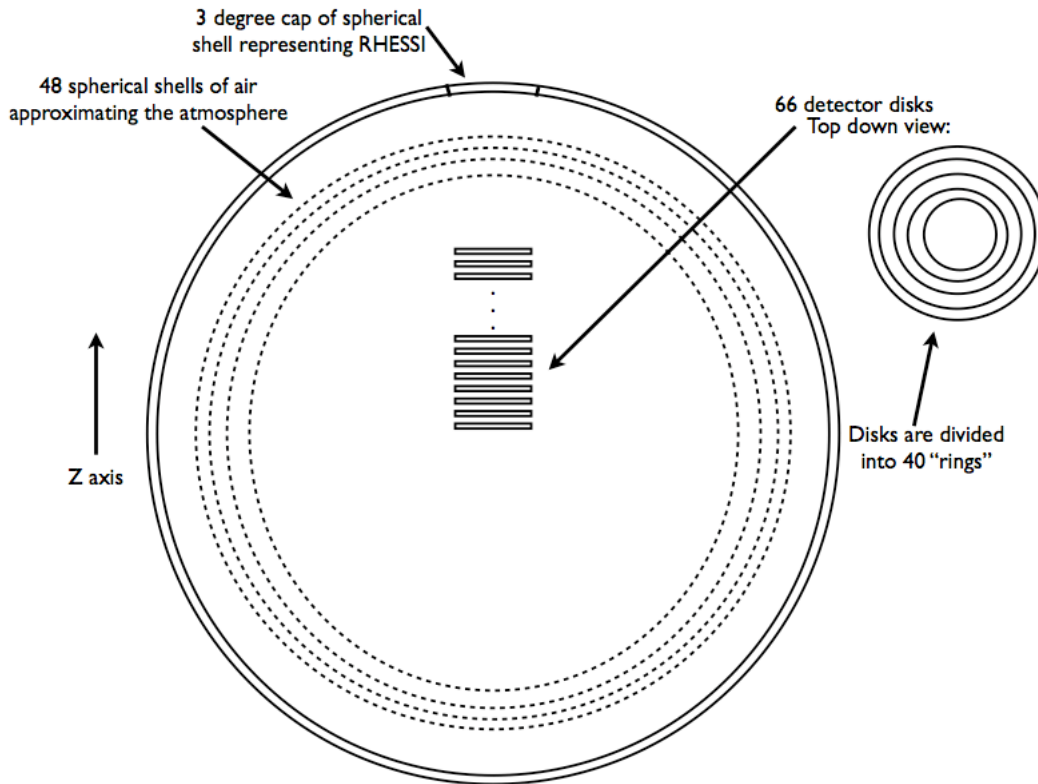


Figure 13: A schematic of the atmospheric mass model, not drawn to scale.

The mass model also included a spherical shell of radius 6972.12 km representing the

RHESSI satellite. The photons that crossed the 3 degree cap of this sphere with energies >50 keV were interpreted as having reached RHESSI. The flux through the area of the 3 degree spherical cap was divided by the known RHESSI sensitivity ($0.15 \frac{\text{counts}}{\text{cm}^2}$ for photons with energies > 100 keV), resulting in a constant of proportionality R used to normalize the strength of the simulated TGF to a typical RHESSI TGF.

TGF source altitudes between 7 km and 20 km were chosen. Electrons were initialized at the source altitude (on the z axis) with energies taken from an exponential distribution with a characteristic energy of 7.2 MeV. The initial directions of the electrons were chosen such that their velocity vectors laid inside of a 32 degree opening. The choice of a 32 degree beam angle was influenced by a simulation of the RREA process carried out by Dwyer (2003). The simulation assumed a uniform, vertical electric field, thus producing the narrowest possible electron beam.

Bremsstrahlung photons were produced via collisions between the electrons and the air. The energy of each photon and the angle made between the photon's direction of motion and the z axis were binned and recorded for every photon that entered a ring. At the the end of the program, the spectra for each ring was written to file for each angular bin.

The photon flux at each ring was calculated by summing up all of the counts in a particular ring with energies > 300 keV, dividing by the effective area, and then multiplying by R. The effective area is a function of angle, since photons coming from different angles have more or less area to impact; The formula used to calculate the effective area was:

$$A_{effective} = \sum_{i=1}^{18} (A_{side} \text{Sin}(10i) + A_{top} \text{Cos}(10i)) \frac{n_i}{n_{total}}$$

In this formula, A_{side} is the area of a ring seen from the side, while A_{top} is the area seen from the top. n_i is the number of counts in the i^{th} angular bin (there are eighteen 10 degree bins), and n_{total} is the total number of counts in all of the angular bins.

The photon fluxes at the Z=13.5 km ring were found as a function of the horizontal distance from the z axis. The horizontal distance of the first ring to go below the sensitivity of the ADELE instrument was defined as the "maximum radius of detectability" (MRD).

3 Results

From the first simulation, the sensitivity of ADELE to a TGF event was found to be 0.14 $\frac{counts}{cm^2}$ for photons with energies >300 keV. Thus, any ring with a flux value of 0.14 $\frac{counts}{cm^2}$ or more would correspond to a region of space in which ADELE should have detected a TGF. The flux values for the rings were determined by the second simulation, and are represented in the contour plot in Fig. 14 for a TGF source altitude of 16 km. All regions to the left and above the 0.14 $\frac{counts}{cm^2}$ contour are "detectable" regions for ADELE.

The R coordinate of the intersection of the dashed line at Z = 13.5 km (the airplane's altitude) with the 0.14 $\frac{counts}{cm^2}$ contour is taken to be the maximum radius of detectability (MRD). Figure 15 shows the MRD as a function of TGF source altitude. The solid line was produced by normalizing the TGF strength to the strength of a typical RHESSI TGF. In other words, the scale factor relating the flux at the RHESSI detector in the simulation to the known RHESSI flux for typical TGFs was used to scale the flux values at each ring. The dashed line was generated by normalizing the 15 km TGF to a typical RHESSI TGF,

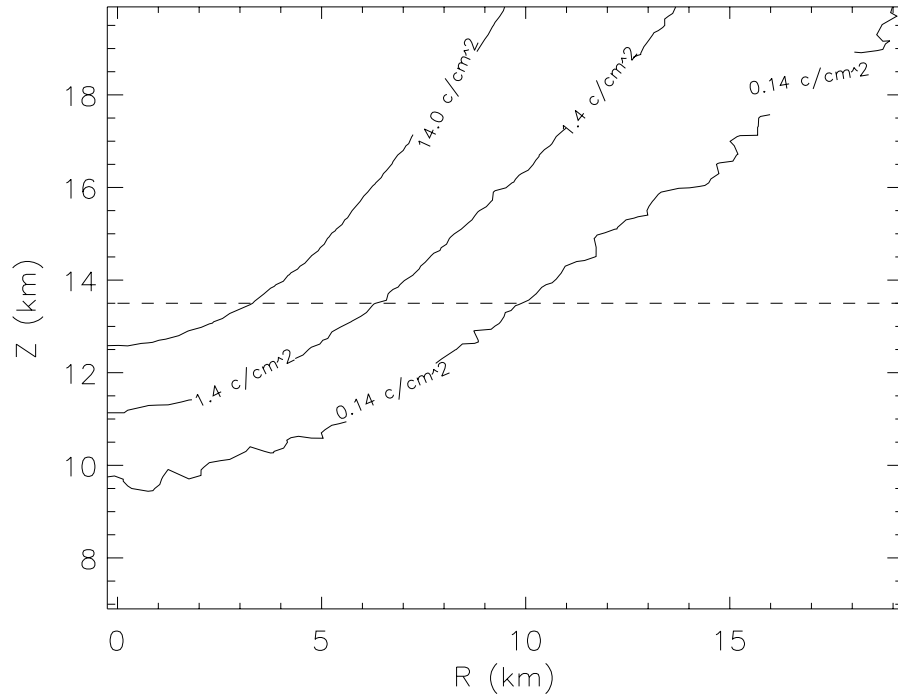


Figure 14: Contour plot showing contours of constant flux in the R-Z plane for a TGF altitude of 16 km. The dashed line at $Z=13.5$ km represents the altitude of the airplane.

and using that normalization for all of the other TGFs. Therefore the dashed line can be interpreted as the MRD as a function of TGF altitude, assuming that the TGF at every altitude is equally luminous as the TGF at 15 km.

4 Discussion

Data from the Weatherbug Total Lightning Network (WTLN) and the United States Precision Lightning Network (USPLN) were used to determine the positions of lightning flashes relative to the airplane's position. Since neither network records every single flash, a

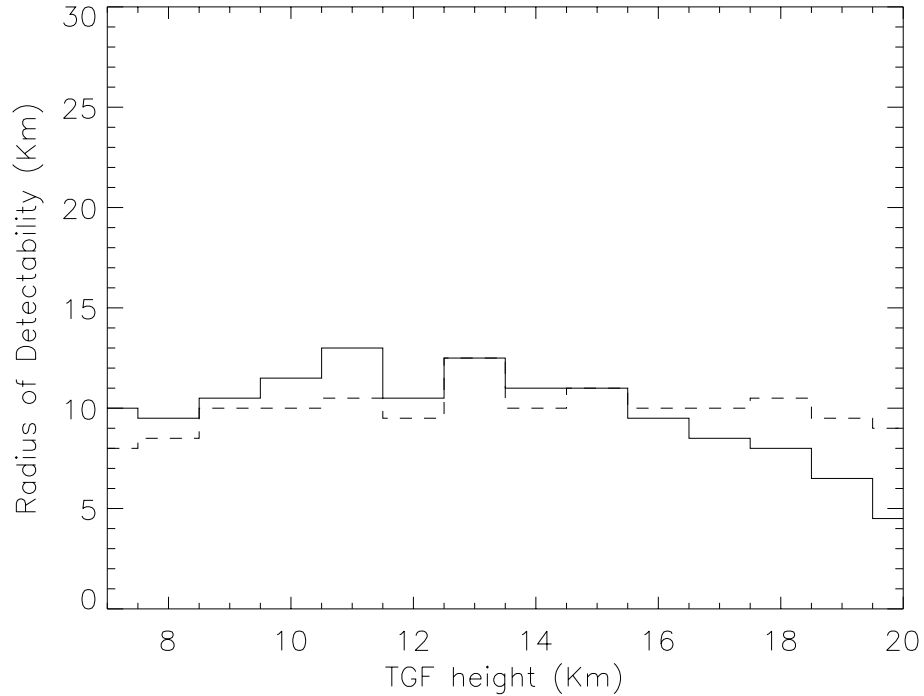


Figure 15: The maximum radii of detectability as a function of TGF source altitude.

restricted set of coincident flashes was compiled. Flashes from both networks were compared and matched if they occurred within 1 millisecond and within 10 km of each other. The list of matches was searched for events that occurred within 10 km of the airplane. The value of 10 km was chosen since it was approximately the average value of MRD from FIGURE. 235 lightning flashes were found within 10 km of the airplane.

Because ADELE did not detect TGFs associated with these flashes, we hypothesize that most lightning is not of the TGF-producing type. It is worth noting that our sample of lightning flashes is limited to lightning from the southeastern United States. Therefore, we cannot make any conclusions about the correlation between lightning and TGFs in other locations around the world, since thunderstorms at different latitudes have different charac-

teristics. Future ADELE campaigns will hopefully take us to more tropical locations where we may diversify our lightning flash sample.

5 References

- Dwyer, J. R., D. M. Smith (2005), *Geophysical Research Letters*, 32, L22804.
- Dwyer, J. R. (2008), *Journal of Geophysical Research*, 113, D10103.
- Dwyer, J. R. (2003), *Geophysical Research Letters*, 30(20), 2055.
- Fishman, G. J. et al. (1994), *Science*, 264, 1313.
- GEANT team (1993), "GEANT - Detector description and simulation tool, CERN Program Library Long Write-up W5013", CERN, Geneva.
- Grefenstette, B. W., D. M. Smith, J. R. Dwyer, G. J. Fishman (2008), *Geophysical Research Letters*, 35, L06802.
- Grefenstette, B. W., D. M. Smith, B. J. Hazelton, L. I. Lopez (2009), *Journal of Geophysical Research*, 114, A02314.
- Inan, U. S., S. C. Reising (1996), *Geophysical Research Letters*, 23(9), 1017.
- McCarthy, M., G. K. Parks (1985), *Geophysical Research Letters*, 12(6), 393.
- Moss, G. D., V. P. Pasko, N. Liu, G. Veronis (2006), *Journal of Geophysical Research*, 111, A02307.

Parks, G. K. et al. (1981), *Geophysical Research Letters*, 8(11), 1176.

Smith, D. M. et al. (2005), *Science*, 307, 1085.

Wilson, C.T.R. (1925), *Mathematical Proceedings of the Cambridge Philosophical Society*, 22, 534.